Graphene/MoS_2 heterostructure: a robust mid-infrared optical modulator for Er^{3+}-doped ZBLAN fiber laser

Pinghua Tang (唐平华)[1], Yue Tao (陶 月)[1], Yuliang Mao (毛宇亮)[1], Man Wu (吴 熳)[2], Zongyu Huang (黄宗玉)[1], Shengnan Liang (梁胜男)[1], Xinhang Chen (陈新行)[1], Xiang Qi (祁 祥)[1,*], Bin Huang (黄 斌)[2], Jun Liu (刘 军)[3], and Chujun Zhao (赵楚军)[2,]**

[1]*Hunan Key Laboratory for Micro-Nano Energy Materials and Devices, School of Physics and Optoelectronics, Xiangtan University, Xiangtan 411105, China*

[2]*Key Laboratory for Micro-/Nano-Optoelectronic Devices of Ministry of Education, School of Physics and Electronics, Hunan University, Changsha 410082, China*

[3]*SZU-NUS Collaborative Innovation Center for Optoelectronic Science & Technology, Key Laboratory of Optoelectronic Devices and Systems of Ministry of Education and Guangdong Province, College of Optoelectronic Engineering, Shenzhen University, Shenzhen 518060, China*

**Corresponding author: xqi@xtu.edu.cn; **corresponding author: cjzhao@hnu.edu.cn*

Received September 23, 2017; accepted November 10, 2017; posted online January 26, 2018

We have prepared the graphene/MoS_2 heterostructure by a hydrothermal method, and presented its nonlinear absorption parameters and application as a nonlinear optical modulator in the mid-infrared region. Using the nonlinear optical modulator, stable passively *Q*-switched operation of an Er^{3+}-doped ZrF_4-BaF_2-LaF_3-AlF_3-NaF (ZBLAN) fiber laser at ~2.8 μm can be obtained. The *Q*-switched Er^{3+}-doped ZBLAN fiber laser can yield per-pulse energy up to 2.2 μJ with the corresponding pulse width and pulse repetition rate of 1.9 μs and 45 kHz, respectively. Our results indicate that the graphene/MoS_2 heterostructure can be a robust optical modulator for pulsed lasers in the mid-infrared spectral range.

OCIS codes: 160.4330, 140.3070, 140.3540.
doi: 10.3788/COL201816.020012.

Two-dimensional (2D) materials offer a platform that allows the creation of heterostructures with unique and unprecedented properties to play an important role in modern electronic devices, and optoelectronic devices, etc.[1]. 2D nanomaterials, such as graphene and molybdenum disulfide (MoS_2), possess excellent nonlinear optical response as a nonlinear optical modulator, which have attracted considerable attention in pulsed laser generation[2]. To date, graphene as an optical modulator has successfully been used to generate *Q*-switched and mode-locked pulses in fiber lasers and solid-state lasers with the operating waveband coverage from near-infrared to mid-infrared[3–5]. However, the relatively weak optical response (2.3% absorption with monolayer graphene) in a widely spectral region limits its application[6]. Although the absorption intensity in graphene can be enhanced by various approaches, such as employing twisted bilayer graphene[6], graphene plasmons[7], and a microcavity[8], unwanted nonsaturable losses will rise. Motived by the progress of graphene, many other graphene-like 2D materials, such as a topological insulator[9–12], black phosphorus[13–17], gold nanorods[18,19], and transition-metal dichalcogenides (TMDCs)[20–24], have been explored as an optical modulator to achieve pulsed lasers.

MoS_2, a typical TMDC, exhibits great potential in optoelectronic applications for its tunable bandgaps and strong light–matter interaction[25]. Unlike semi-metallic graphene, MoS_2 is a semiconductor with the band gap changing from indirect to direct when the thickness is reduced to a monolayer, and this indirect-to-direct gap transition sparks off great enhancement in the photo-response[26]. Moreover, MoS_2 exhibits strong light–matter interaction in association with Van Hove singularities in the density of states[27]. Recently, using MoS_2 as the optical modulator, researchers have realized broadband *Q*-switching (Q-S) and mode-locking[20,21,28–33]. However, MoS_2 alone used as an optical modulator suffers from the relatively long relaxation time of the intraband excitation in comparison with graphene[34] and the rapid recombination of the photo-excited electron–hole pairs[26].

Fortunately, triggered by the progress of the nanocomposite, researchers have explored a new functional material, namely, the graphene/MoS_2 heterostructure, which succeeds in the advantages of graphene and MoS_2, while it overcomes their disadvantages[25,35]. Studies have demonstrated that the advantages of ultrafast relaxation, broadband response from graphene, and the strong light–matter interaction from MoS_2 can be combined together by the graphene/MoS_2 heterostructure[25]. Moreover, photo-excited electron-hole pairs produced by MoS_2 can be easily separated at the MoS_2 and graphene interfaces in these heterostructures[26]. These excellent photoelectric properties make the graphene/MoS_2 heterostructure a promising optical modulator. Recently, Zhao *et al.*[36] and Jiang *et al.*[25] have realized both Q-S and mode-locking at 1 and 1.5 μm, using the graphene/MoS_2 heterostructure as the optical modulator, respectively.

However, their researches only focus on the near-infrared region.

In this letter, we report the nonlinear absorption parameters of the graphene/MoS_2 heterostructure, and its application for an optical modulator in the mid-infrared region. Using the graphene/MoS_2 heterostructure as an optical modulator, stable passively Q-switched operation of the Er^{3+}-doped ZrF_4-BaF_2-LaF_3-AlF_3-NaF (ZBLAN) fiber laser at ~2.8 μm can be obtained. At an incident pump power of 4.1 W, the Q-switched Er^{3+}-doped ZBLAN fiber laser yielded per-pulse energy of 2.2 μJ with the corresponding pulse width and pulse repetition rate of 1.9 μs and 45 kHz, respectively.

The graphene/MoS_2 heterostructure was prepared by a typical hydrothermal method. First, a graphene oxide (GO) precursor was synthesized from 170 mg of graphite powder by a modified Hummer's method using a mixture of H_2SO_4, P_2O_5, and $KMnO_4$. Secondly, the as-prepared GO was dissolved in 40 mL of deionized water under vigorous stirring for 1 h to get a homogeneous suspension. Next, 300 mg of $Na_2MoO_4 \cdot 2H_2O$ was added into the above GO aqueous solution with stirring for another 2 h at room temperature. Then, the solution was adjusted to a pH of 6.5 with 0.1 M NaOH. 800 mg of L-cysteine was dissolved in 80 mL deionized water and then transferred into a 100 mL Teflon-lined stainless steel autoclave and heated at 240°C for 24 h. The resulting black precipitates were collected by centrifugation and were washed by deionized water and ethanol for three times. The collected powders were dried in a vacuum oven at 80°C for 24 h. The dried powders were annealed at 800°C for 2 h with a heating rate of 5°C/min in a stream of 10% hydrogen in nitrogen flowing at 200 sccm to carbonize the polydopamine and crystallize MoS_2. Finally, the obtained graphene/MoS_2 heterostructure with a 1:1 molar ratio of MoS_2 to graphene was designated.

Figure 1(a) displays the typical scanning electron microscope (SEM) image of the as-prepared graphene/MoS_2 heterostructure sample. It is obvious that large scale MoS_2 nanosheets with lateral dimensions are well supported on the graphene platform. To further characterize the structure of the sample, X-ray diffraction (XRD) and Raman spectroscopy measurements were performed. Figure 1(b) shows the typical XRD pattern of the as-prepared graphene/MoS_2 heterostructure sample, in which the diffraction lines can be readily indexed to those of the 2H-MoS_2 phase (JCPDF card No. 37-1492). The consistency between them confirms the existence of MoS_2 in the composite. Diffraction signals of graphene can hardly be discerned in the present XRD pattern of the graphene/MoS_2 heterostructure due to the weak diffraction intensity and low crystallinity of graphene. However, graphene in the composite can be identified by the Raman spectrum, as shown in Fig. 1(c). Two strong peaks located at 1353 and 1602 cm^{-1}, which can be indexed to the D band and G band of graphene, are characteristic Raman signals of graphene. Additionally, the in-plane Mo-S phonon mode (E^1_{2g}), out-of-plane Mo-S mode

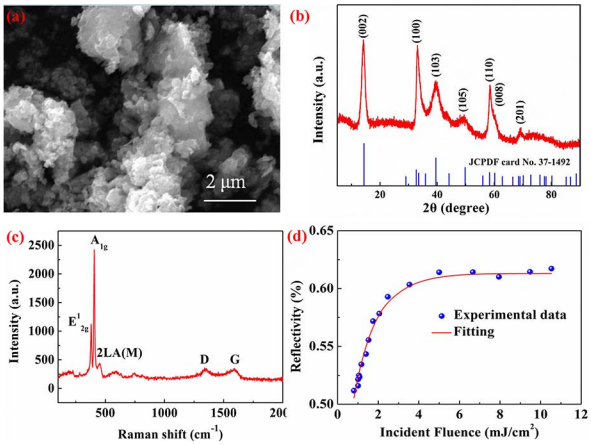

Fig. 1. Characterizations of the graphene/MoS_2 heterostructure. (a) SEM image, (b) XRD pattern, and (c) Raman spectrum of the graphene/MoS_2 heterostructure sample. (d) The measured nonlinear power-dependent reflectivity of the graphene/MoS_2 heterostructure modulator.

(A_{1g}), and second-order Raman scattering 2LA(M) are also observed at 380, 407, and 460 cm^{-1}, respectively.

In order to construct the graphene/MoS_2 heterostructure modulator, the as-prepared graphene/MoS_2 heterostructure sample was transferred onto a gold mirror (reflectivity >95% at ~2.8 μm). We would like to mention that the gold mirror acting as a substrate can ensure efficient heat removal of the modulator since it has good heat conducting properties. Based on a balanced twin-detector measurement technique with a home-built optical parametric oscillator at around 2.8 μm acting as a pump source, the nonlinear absorption of the constructed graphene/MoS_2 heterostructure modulator was measured. Figure 1(d) shows the measured nonlinear power-dependent reflectivity of the graphene/MoS_2 heterostructure modulator. By fitting the data with the formula,

$$R(I) = 1 - \alpha_s \cdot \exp(-I/I_{\text{sat}}) - \alpha_{\text{ns}}, \tag{1}$$

where R is the reflectivity, α_s is the modulation depth, I is the incident pulse energy, I_{sat} is the saturable energy density, and α_{ns} is the nonsaturable loss, one can obtain the modulation depth, saturable energy density, and nonsaturable loss, which are about 22%, 1.1 mJ/cm^2, and 38.7%, respectively. The larger modulation depth and larger saturable energy density compared to graphene indicate that graphene/MoS_2 heterostructure modulator has greater potential for obtaining stable and high-energy pulsed lasers.

The schematic diagram of our constructed graphene/MoS_2 heterostructure modulator Q-switched Er^{3+}-doped ZBLAN fiber laser is depicted in Fig. 2. A commercially available 40 W fiber-coupled laser diode operating at 975 nm with a core diameter of 105 μm and a numerical aperture (NA) of 0.22 was employed to pump the gain fiber. The pump beam was collimated by a lens L1 (N-BK7,

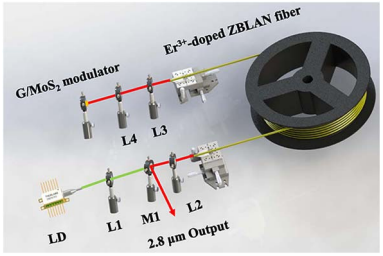

Fig. 2. Experimental setup of the graphene/MoS_2 heterostructure Q-switched Er^{3+}-doped ZBLAN fiber laser. G/MoS_2, graphene/MoS_2 heterostructure.

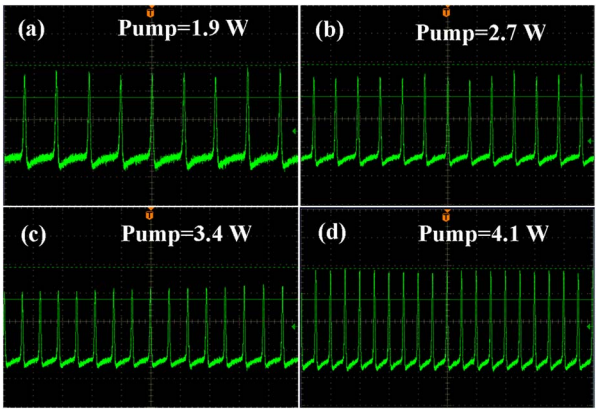

Fig. 3. Oscilloscope traces of the Q-switched pulses with different incident powers. (a), (b), (c), and (d) with an incident pump power of 1.9, 2.7, 3.4, and 4.1 W, respectively.

coating-B, $f = 25.4$ mm) and focused by another lens L2 (CaF_2, uncoated, $f = 50$ mm), with the spot diameter of about 207 μm on the fiber end face. The gain fiber is a 3 m double clad Er^{3+}-doped ZBLAN fiber (FiberLabs, Japan) with the dopant concentration of 6 mol. % and has a core diameter of 32 μm with a NA of 0.12. The first cladding configuration of the fiber is octagonal with a diameter of 300 μm across the circular cross section, and a NA of >0.5 to guarantee efficient pump coupling. The second cladding diameter of the fiber is 425 μm. The intrinsic loss of the fiber at 980 nm is 3–4 dB/m. One fiber end at the pump incident side was perpendicular-cleaved, and its facet functioned as an output coupler with the aid of 4% Fresnel reflection. The other end of the fiber was cleaved at an angle of 8° to avoid parasitic lasing. The intracavity laser was collimated by a lens L3 (CaF_2, uncoated, $f = 20$ mm) and focused by another lens L4 (CaF_2, uncoated, $f = 25.4$ mm) with a spot diameter of about 207 μm on the graphene/MoS_2 heterostructure modulator. The output laser beam is separated from the pump beam by a 45° placed dichroic mirror M1 (high reflectivity at the lasing wavelength of 2.8 μm and high transmission at the pump wavelength of 975 nm). To ensure efficient heat removal, both ends of the fiber were mounted in a V-groove engraved aluminum heat sink. The output pulse trains were recorded by a 500 MHz digital oscilloscope (Tektronix, DPO3054) together with an infrared InAs detector with a rise time of ~3 ns. The output spectra were monitored by a high-resolution monochromator (Princeton, Acton SP2300). The signal-to-noise ratio (SNR) was analyzed by a radio-frequency (RF) spectral analyzer (Agilent, N9322C).

When the incident pump power was lower than 1.9 W, the Q-S was chaotic. Beyond this value, it shifted to a stable Q-S regime. In order to confirm that the Q-switched operation actually resulted from the modulation of the graphene/MoS_2 heterostructure modulator, we deliberately substituted the graphene/MoS_2 heterostructure modulator with a pure gold mirror, and no self-Q-S was observed. Figure 3 shows the recorded oscilloscope traces under different incident pump powers. As shown in Fig. 3, one can see the pulse repetition rate became gradually larger, as the incident pump power increased. This typical feature of passive Q-S further verifies the role of the graphene/MoS_2 heterostructure modulator.

The specific pulse width and pulse repetition rate with respect to the incident pump power are shown in Fig. 4(a). The pulse width decreased from 3.0 μs at an incident pump power of 1.9 W to 1.9 μs at an incident pump power of 4.1 W, while the corresponding repetition rate increased from 23 to 45 kHz. Figure 4(b) shows the average output power and per-pulse energy versus incident pump power. At an incident pump power of 4.1 W, the average output power reached up to 100 mW with the corresponding per-pulse energy of 2.2 μJ and the optical-optical conversion efficiency of 2.4%. The low efficiency could be attributed to the large insert loss of the graphene/MoS_2 heterostructure modulator. At an average output power of 100 mW, the graphene/MoS_2 heterostructure modulator Q-switched Er^{3+}-doped ZBLAN

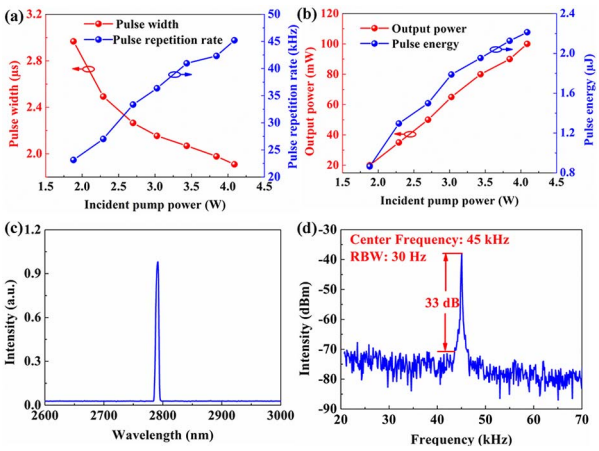

Fig. 4. Output characteristics of the graphene/MoS_2 heterostructure Q-switched Er^{3+}-doped ZBLAN fiber laser. (a) Pulse width and pulse repetition rate and (b) output power and per-pulse energy versus incident pump power; (c) output spectrum and (d) RF spectrum at the average output power of 100 mW.

fiber laser operated at a 2791 nm wavelength with the SNR of 33 dB, as shown in Figs. 4(c) and 4(d), respectively. The large SNR indicates that the laser operated in a stable Q-S regime. We would like to mention that optical damage of the graphene/MoS_2 heterostructure saturable absorber (SA) was observed when the incident pump power was beyond 4.1 W.

In conclusion, nonlinear absorption parameters of the graphene/MoS_2 heterostructure and its application for an optical modulator in the mid-infrared region are reported. Nonlinear absorption measurement indicates that the constructed graphene/MoS_2 heterostructure modulator has a large modulation depth of ~22% and a large saturable energy density of ~1.1 mJ/cm^2, which are beneficial to obtaining stable and high-energy pulsed lasers. Using the graphene/MoS_2 heterostructure as an optical modulator, stable passively *Q*-switched operation of the Er^{3+}-doped ZBLAN fiber laser at ~2.8 μm with an SNR of 33 dB was achieved. At an incident pump power of 4.1 W, the *Q*-switched Er^{3+}-doped ZBLAN fiber laser yielded per-pulse energy of 2.2 μJ with the corresponding pulse width and pulse repetition rate of 1.9 μs and 45 kHz, respectively. These results show the potential of the graphene/MoS_2 heterostructure for pulsed lasers in the mid-infrared spectral range.

This work was supported by the China Postdoctoral Science Foundation (No. 2017M620349), the National Natural Science Foundation of China (Nos. 61605166, 11374251, and 61505124), the Research Foundation of Education Bureau of Hunan Province, China (No. 17C1519), and the Program for Changjiang Scholars and Innovative Research Team in University of China (No. IRT 17R91).

References

1. J. M. Hamm and O. Hess, Science **340**, 1298 (2013).
2. Z. P. Sun, A. Martinez, and F. Wang, Nat. Photon. **10**, 227 (2016).
3. Q. L. Bao, H. Zhang, Y. Wang, Z. H. Ni, Z. X. Shen, K. P. Loh, and D. Y. Tang, Adv. Funct. Mater. **19**, 3077 (2009).
4. Z. P. Sun, T. Hasan, F. Torrisi, D. Popa, G. Privitera, F. Q. Wang, F. Bonaccorso, D. M. Ferrari, and A. C. Ferrari, ACS Nano **4**, 803 (2010).
5. C. Wei, X. Zhu, F. Wang, Y. Xu, K. Balakrishnan, F. Song, R. A. Norwood, and N. Peyghambarian, Opt. Lett. **38**, 3233 (2013).
6. J. B. Yin, H. Wang, H. Peng, Z. J. Tan, L. Liao, L. Lin, X. Sun, A. L. Koh, Y. L. Chen, H. L. Peng, and Z. F. Liu, Nat. Commun. **7**, 10699 (2016).
7. F. H. L. Koppens, D. E. Chang, and F. J. García de Abajo, Nano Lett. **11**, 3370 (2011).
8. F. Marco, U. Alexander, P. Andreas, L. Govinda, U. Karl, D. Hermannn, K. Pavel, M. A. Aaron, S. Werner, S. Gottfried, and M. Thomas, Nano Lett. **12**, 2773 (2012).
9. C. J. Zhao, H. Zhang, X. Qi, Y. Chen, Z. T. Wang, S. C. Wen, and D. Y. Tang, Appl. Phys. Lett. **101**, 201106 (2012).
10. P. H. Tang, X. Q. Zhang, C. J. Zhao, Y. Wang, H. Zhang, D. Y. Shen, S. C. Wen, D. Y. Tang, and D. Y. Fan, IEEE Photon. J. **5**, 1500707 (2013).
11. Z. C. Luo, M. Liu, H. Liu, X. W. Zheng, A. P. Luo, C. J. Zhao, H. Zhang, S. C. Wen, and W. C. Xu, Opt. Lett. **38**, 5212 (2013).
12. J. S. Lee, M. W. Jung, J. Koo, C. Chi, and J. H. Lee, IEEE J. Sel. Top. Quantum Electron. **21**, 264 (2015).
13. Y. Chen, G. B. Jiang, S. Q. Chen, Z. N. Guo, X. F. Yu, C. J. Zhao, H. Zhang, Q. L. Bao, S. C. Wen, D. Y. Tang, and D. Y. Fan, Opt. Express **23**, 12823 (2015).
14. J. Sotor, G. Sobon, W. Macherzynski, P. Paletko, and K. M. Abramski, Appl. Phys. Lett. **107**, 051108 (2015).
15. Z. C. Lou, M. Liu, Z. N. Guo, X. F. Jiang, A. P. Luo, C. J. Zhao, X. F. Yu, W. C. Xu, and H. Zhang, Opt. Express **23**, 20030 (2015).
16. Z. P. Qin, G. Q. Xie, C. J. Zhao, S. C. Wen, P. Yuan, and L. J. Qian, Opt. Lett. **41**, 56 (2016).
17. X. Wang, Z. F. Wang, Y. G. Wang, L. Li, G. W. Yang, and J. P. Li, Chin. Opt. Lett. **15**, 011402 (2017).
18. Z. Kang, Y. Xu, L. Zhang, Z. X. Jia, L. Liu, D. Zhao, Y. Feng, G. S. Qin, and W. P. Qin, Appl. Phys. Lett. **103**, 041105 (2013).
19. H. T. Huang, M. Li, L. Wang, X. Liu, D. Y. Shen, and D. Y. Tang, IEEE Photon. J. **7**, 4501210 (2015).
20. H. Zhang, S. B. Lu, J. Zheng, J. Du, S. C. Wen, D. Y. Tang, and K. P. Loh, Opt. Express **22**, 7249 (2014).
21. R. I. Woodward, R. C. T. Howe, G. Hu, F. Torrisi, M. Zhang, T. Hasan, and J. R. Kelleher, Photon. Res. **3**, A30 (2015).
22. C. Wei, H. Y. Luo, H. Zhang, C. Li, J. T. Xie, J. F. Li, and Y. Liu, Laser Phys. Lett. **13**, 105108 (2016).
23. Z. Q. Luo, Y. Y. Li, M. Zhong, Y. Z. Huang, X. J. Wan, J. Peng, and J. Weng, Photon. Res. **3**, A79 (2015).
24. Z. C. Tiu, H. Ahmad, A. Zarei, and S. W. Harun, Chin. Opt. Lett. **14**, 041901 (2016).
25. Y. Q. Jiang, L. L. Miao, G. B. Jiang, Y. Chen, X. Qi, X. F. Jiang, H. Zhang, and S. C. Wen, Sci. Rep. **5**, 16372 (2015).
26. Z. Y. Huang, W. J. Han, X. J. Liu, X. Qi, and J. X. Zhong, Ceram. Int. **40**, 11971 (2014).
27. L. Britnell, R. M. Ribeiro, A. Eckmann, R. Jalil, B. D. Belle, A. Mishchenko, Y. J. Kim, R. V. Gorbachev, T. Georgiou, S. V. Morozov, A. N. Grigorenko, A. K. Geim, C. Casiraghi, A. H. Castro Neto, and K. S. Novoselov, Science **340**, 1311 (2013).
28. J. Du, Q. K. Wang, G. B. Jiang, C. W. Xu, C. J. Zhao, Y. J. Xiang, Y. Chen, S. C. Wen, and H. Zhang, Sci. Rep. **4**, 6346 (2014).
29. Z. Q. Luo, Y. Z. Huang, M. Zhong, Y. Y. Li, J. Y. Wu, B. Xu, H. Y. Xu, Z. P. Cai, J. Peng, and J. Weng, J. Lightwave Technol. **32**, 4679 (2014).
30. H. D. Xia, H. P. Li, C. Y. Lan, C. Li, X. X. Zhang, S. J. Zhang, and Y. Liu, Opt. Express **22**, 17341 (2014).
31. J. Ren, S. X. Wang, Z. C. Cheng, H. H. Yu, H. J. Zhang, Y. X. Chen, L. M. Mei, and P. Wang, Opt. Express **23**, 5607 (2015).
32. L. C. Kong, G. Q. Xie, P. Yuan, L. J. Qian, S. X. Wang, H. H. Yu, and H. J. Zhang, Photon. Res. **3**, A47 (2015).
33. X. Zou, Y. X. Leng, Y. Y. Li, Y. Y. Feng, P. X. Zhang, Y. Hang, and J. Wang, Chin. Opt. Lett. **13**, 081405 (2015).
34. K. P. Wang, J. Wang, J. T. Fan, L. Mustafa, A. O'Neill, D. Fox, Y. Y. Feng, X. Y. Zhang, B. X. Jiang, Q. Z. Zhao, H. Z. Zhang, J. N. Coleman, L. Zhang, and W. J. Blau, ACS Nano **7**, 9260 (2013).
35. W. J. Zhang, C. P. Chuu, J. K. Huang, C. H. Chen, M. L. Tsai, Y. H. Chang, C. T. Liang, Y. Z. Chen, Y. L. Chueh, J. H. He, M. Y. Chou, and L. J. Li, Sci. Rep. **4**, 3826 (2014).
36. G. Zhao, J. Hou, Y. Z. Wu, J. L. He, and X. P. Hao, Adv. Opt. Mater. **3**, 937 (2015).